Bipolar spindle formation is a fast, irreversible process requiring Kinesin-5 crosslinking and sliding modalities.

Allen Leary[1], Elena Nazarova[1], Shannon Sim[1], Kristy Shulist[1], Paul Francois[2,3] and Jackie Vogel*[1,2]

[1]Department of Biology, McGill University, Montreal QC Canada

[2]Integrated Quantitative Biology Initiative, McGill University, Montreal QC Canada

[3]Department of Physics, McGill University, Montreal QC Canada

*Author for correspondence: jackie.vogel@mcgill.ca

Running title: Fast, irreversible bipolar spindle formation

Keywords: Kinesin-5, spindle, microtubules, mitosis

Short summary:

Abstract

Formation of a bipolar spindle is the first step in the accurate segregation of chromosomes during cell division. Kinesin-5 is an highly conserved motor protein required to form the bipolar spindle, and can both cross-link and slide anti-parallel microtubules. Yet how these two modalities combine to form a bipolar spindle remains unclear. In this study, we report that Kinesin-5 cross-linking and sliding of microtubules have distinct roles in the fast, irreversible formation of a stable bipolar spindle in budding yeast. We report that mutations in Kinesin-5 orthologs that impair microtubule sliding do not reduce the velocity of pole separation or delay the onset of spindle formation. Using electron tomography models, we show that microtubule pairs in the initial monopolar state have short overlaps and intersect at a high angle, and are unsuited to ensemble kinesin-5 sliding. However, this highly coupled system can support a maximal extension of cross-linked microtubules consistent with the length of nascent bipolar spindles. Finally, we find microtubule sliding by kinesin-5 determines both the equilibrium length of the nascent bipolar spindle and reduces fluctuations in spindle length. We propose that kinesin-5 crosslinks anti-parallel microtubules to first form the bipolar spindle and then slides these microtubules apart to maintain a stable bipolar state at a stereotyped length.

Introduction

Accurate segregation of chromosomes into daughter cells requires a stable bipolar spindle. The stability of the mitotic spindle is based in a stereotyped design blueprint composed of two spindle poles on which microtubules (MT) are assembled. The first and most critical step in mitosis is the transition from a monopolar state to a bipolar state. In the new bipolar spindle, some MTs from opposing poles crosslink to form a set of stabilizing inter-polar MTs (ipMTs) while other MTs probe for, and attach to, the centromeres of sister chromatids. The new bipolar spindle is subject to myriad opposing, destabilizing forces arising from MT and chromosomes that could cause a collapse to the monopolar state. Indeed, mutations in kinesin-5 and Ase1 that disrupt MT cross-linking cause spindle collapse. Two related and unresolved questions are how the organization of MTs in the monopolar state support the production of the forces required separate the spindle poles, and why the nascent bipolar spindle does not collapse.

The formation of a bipolar spindle depends on the conserved Kinesin-5 family of plus ended motor proteins. Kinesin-5 is organized as a homo-tetramer and can both crosslink anti-parallel MTs as well as slide them apart[1]. Studies to date have focused on Kinesin-5's role in the maintenance of the bipolar spindle by virtue of its pushing forces which oppose the contractile forces enacted on the spindle by minus ended Kinesin 14 and dynein. Budding yeast has two kinesin-5 orthologs: Cin8 and Kip1[2,3]. Although Cin8 and Kip1 have been reported as being functionally redundant for bipolar spindle formation, Cin8 is thought to have the greater role in spindle assembly as cin8Δ cells delay in metaphase and require a functional spindle assembly checkpoint. Yet bipolar spindle formation, the initial transition from a monopolar state with duplicated spindle poles to a stable bipolar spindle, cannot be explained by mechanisms for bipolar spindle maintenance. How kinesin-5 drives this monopolar to bipolar transition through the MT architecture of the monopolar state is remains unclear.

In this study we employ the simplicity of the budding yeast mitotic spindle to investigate the properties of the monopolar to bipolar transition and the contributions of both Kinesin-5 crosslinking and sliding modalities. We used confocal microscopy and a cre-lox recombinase-based fluorophore-switching system to spectrally separate spindle poles below the diffraction limit. We track the poles as point like objects before, during and after the monopolar to bipolar transition. Pole separation traces capture dynamic information for the transition, allowing us to measure for the first time the velocity of the poles as they separate as well as the stability of the nascent bipolar spindle. The transition is fast and irreversible, with an average pole separation velocity of 17± 4 nm sec^{-1}, making it one of the fastest steps in spindle assembly. We report that mutations inhibiting kinesin-5 MT sliding do not significantly change pole separation velocities. Using 3D electron tomography, we show that the MT structure of the initial monopolar state is comprised of short, high angle MT pairings that are unsuited to ensemble kinesin-5 sliding. However, this highly coupled system supports the maximal extension of cross-linked MTs required to achieve the bipolar state as measured for WT cells. However, we find that that the length and stability of the nascent bipolar spindle is dependent on Kinesin-5 MT sliding. We propose that while kinesin-5 sliding does not specifically contribute to the monopolar to bipolar transition, both kinesin-5 sliding and crosslinking are required to form a stereotyped, stable bipolar spindle.

Results

The monopolar to bipolar spindle transition is fast and irreversible

Previous studies in both fission yeast[4] and budding yeast[5] proposed that Cin8 sliding is dispensable for the monopolar to bipolar transition, but the velocity and irreversibility of the

transition in the presence or absence of Kinesin-5 sliding has not yet been measured. In order to quantify the velocity and irreversibility of the formation of a bipolar spindle, we first defined spindle formation as a transition that links the monopolar spindle state with duplicated but unseparated spindle poles and an average length of ~200 nm (pole to pole distance) to the bipolar spindle state. Prior to anaphase, we found the length distribution of bipolar spindles in a population of WT cells to be 800 - 2100 nm[6,7] , suggesting that during the transition the length of the spindle increases by at least 4-fold. To measure this dynamic process, we employed a fluorophore switching technique[8,9], to spectrally separate the pre-existing (old) pole from the newly assembled (new) pole. Spc42, a major component of the central plaque of the spindle pole was tagged with a Cre-Lox recombinase system that recombines out an in-frame mCherry tag and leaves an in-frame EGFP tag (Fig 1a). As a result, cells have old poles labelled with Spc42-mCherry and new poles labelled with Spc42-eGFP, providing high spatio-temporal resolution (100 nm/20 seconds) that resolves the displacements of the un-separated spindle poles in the monopolar spindle state as well as during and after the transition (Fig 1b).

Using simultaneous dual camera imaging, we captured dynamic profiles that encompass the monopolar state, the transition and the new bipolar state. These dynamic profiles of asynchronous cells going through the transition when aligned using their start point present a stereotyped profile (Fig 1c). We defined the velocity of bipolar spindle formation as the velocity of pole separation between the points determined as the start and end point of the transition as defined by the local maxima/minima of the acceleration curves of the pole dynamic profiles. Surprisingly, the monopolar to bipolar transition is very fast in WT cells, with a mean velocity of pole separation in WT cells of 17.1 $\pm$ 3.7 nm sec^{-1} (n=18) that approaches the previously reported velocity of Cin8 anti-parallel sliding (17 nm sec^{-1}) measured in vitro[10]. The monopolar to bipolar transition is faster than any other major transition in spindle assembly including fast anaphase (10 -12nm nm sec^{-1})[2]. In addition, we did not observe any instance of a new bipolar

spindle collapsing to the monopolar state, indicating the transition is irreversible. While new bipolar spindles fluctuate in length, we did not observe post-transition lengths less than 600 nm, well above the 200 nm pole to pole distance of a monopolar spindle. We next employed a Cin8 separation of function mutation combined with a kip1Δ deletion to investigate the independent contributions of kinesin-5 microtubule cross-linking and sliding to the velocity and the irreversibility of the monopolar to bipolar transition.

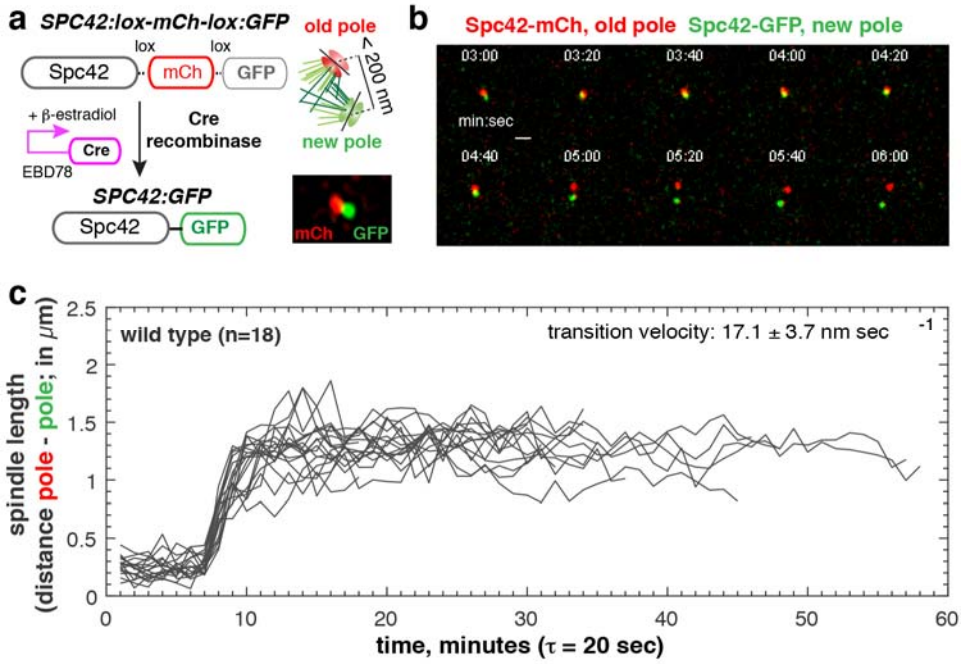

Figure 1: Spindle pole fluorescent-switching technique to characterize the monopolar to bipolar spindle transition in living cells. ***a***. Method for Spc42-mCherry-GFP switching in live cells: in frame mCHERRY is flanked by loxP sites, which allows excision of the mCherry-coding sequence by Cre-recombinase leaving the in frame GFP sequence. The old pole is labelled with mCherry and the new pole with GFP and can be spectrally separated below the diffraction limit. ***b***. Time lapse images of a wild type cell where Spc42-mCh labels the old spindle pole and Spc42-GFP labels the new spindle pole. ***c***. Aligned

traces of WT spindle length dynamics during bipolar spindle formation. For ***b*** and ***c***, time step τ = 20 seconds. Scale bar in ***b***= 1 µm.

Initial separation of the spindle poles is driven by kinesin-5 microtubule crosslinking

Kinesin-5 motor activity relies on its ability to stably associate with MTs[11]. However, mutations that reduce the sliding activity of kinesin-5 while conserving its crosslinking activity have been identified and characterized in vitro, allowing us to investigate each modality individually.

To characterize the contribution of kinesin-5 microtubule sliding to the monopolar to bipolar transition, we first isolated the main driver Cin8's cross-linking modality from its sliding modality using a Cin8 R196K point mutation (Cin8-RK) affecting the α2 helix of the motor domain previously shown to severely reduce motor activity (3% motile MTs vs 20% motile in vitro motility assays)[11]. Cin8-RK had previously showed to be able to form bipolar spindles but the precise velocity and dynamic profiles of the monopolar to bipolar transitions are yet to be characterized. Aligned traces of instantaneous length for the monopolar state, the transition and bipolar state of spindles in WT and the Cin8-RK present remarkably similar profiles (Fig 2 b). We found that the monopolar to bipolar transition in the Cin8-RK mutant is fast, with a mean transition velocity of 16.9± 2.8 nm sec^{-1} n=16 and is not significantly different than the velocity found for WT cells. The monopolar to bipolar transition is also irreversible in Cin8-RK cells. Our results suggest that fast, irreversible formation of a bipolar spindle formation does not depend on anti-parallel microtubule sliding by Cin8.

Kip1 has been found to rescue bipolar spindle formation in the absence of Cin8 and could contribute anti-parallel microtubule sliding in the Cin8-RK mutant. To identify a possible Kip1 sliding contribution to the velocity of pole separation, we deleted the KIP1 gene in the Cin8-RK mutant, and used the Cin8-RK, kip1Δ double mutant to determine if the fast, irreversible transition can be driven by Cin8 crosslinking alone. We found that the mean velocity

of pole separation during the monopolar to bipolar transition to be 17.8± 6.5 nm sec^{-1} in the Cin8-RK kip1Δ mutant (n=12), and not significantly decreased relative to pole separation in WT cells and the Cin8-RK mutant. Together these results suggest that fast, irreversible formation of a bipolar spindle does not require a significant contribution from Kinesin-5 (Cin8 or Kip1) sliding.

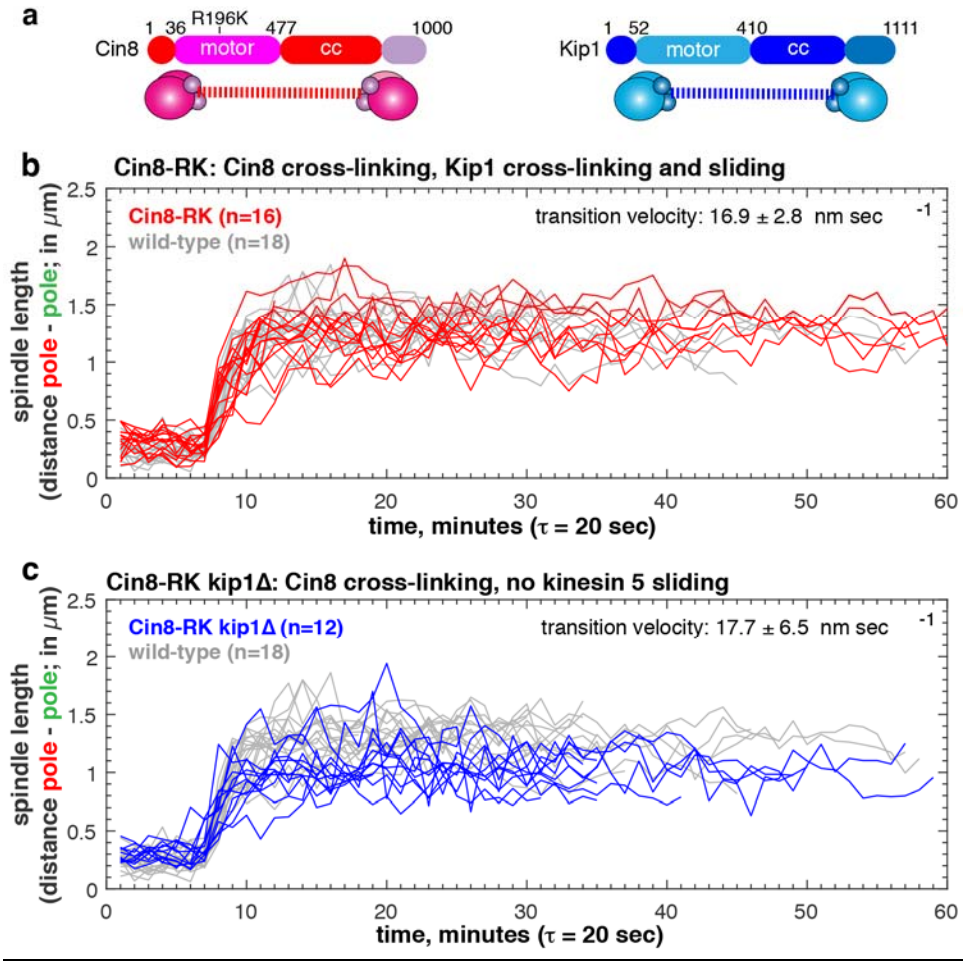

Figure 2: The monopolar to bipolar spindle transition is governed by the cross-linking modality of Kinesin-5. ***a***. Cartoon depicting domains of kinesin-5 orthologs Cin8 and Kip1. ***b***. Plots of spindle length dynamics during bipolar spindle formation in WT cells (grey n=18) and Cin8-RK mutant cells (red n=16). ***c***. Plots of spindle length dynamics during bipolar spindle formation for both WT (grey n=18) and Cin8-RK kip1Δ cells (blue n=12).

Sliding of anti-parallel microtubules by kinesin-5 ensures stability and growth of the new bipolar spindle

The stability of the spindle is essential to form correct chromosome attachments and is the product of the concerted efforts of many highly regulated mitotic actors[12]. Kinesin-5 has been shown to maintain spindle bipolarity by providing a plus ended sliding force[13-15] that counters the minus ended forces from kinesin-14[16]. Our data allow us to investigate the stability of the spindle immediately after the transition to the bipolar state. We therefore wanted to investigate the contribution of kinesin-5 MT sliding and crosslinking to the stability and growth of the nascent bipolar spindle.

To understand how Kinesin-5 contributes to the dynamics of nascent spindles, we first determined if nascent spindles were undergoing net growth immediately following bipolar spindle formation. To address this, we extracted the mean velocity of the instantaneous spindle length traces after the monopolar to bipolar transition (Fig. 3a,c and Fig Suppl). The mean velocities obtained for the rate of elongation of nascent WT and Cin8-RK spindles are similar; respectively 0.211± 0.429 and 0.271±0.393 nm sec^{-1}, however we find that in Cin8-RK, kip1Δ cells the majority of nascent spindles do not elongate (-0.143±0.307 nm sec^{-1}). As a whole the nascent spindle population (WT, Cin8-RK and Cin8-RK kip1Δ) possess a broad distribution of mean velocities centred around 0 ranging from -0.67nm sec^{-1} to 1.2nm sec^{-1} (Fig 3 a, bottom right panel).

Metaphase spindles have been shown to stably grow prior to anaphase[6] and we therefore compared the growth of nascent spindles to the growth of an asynchronous population

of pre-anaphase spindles taken in the same imaging regime. Interestingly, while the rate of growth for the asynchronous population (0.232 ± 0.183 nm sec^{-1}) was similar to the average for nascent WT and Cin8-RK spindles (0.238 ± 0.409 nm sec^{-1}), we found the variations in growth rate is halved and the fraction of spindles undergoing net growth (92.5%) was increased in the asynchronous population relative to nascent WT and Cin8-RK spindles (75%) (Fig.3b,c). The population of later asynchronous WT spindles display a stereotyped elongation regime whilst the nascent spindles exhibit a wider range of mean velocities immediately following monopolar to bipolar spindle transition.

Anaphase onset in WT budding yeast occurs between 2.5-3 µm[17] which is reached through spindle elongation from the nascent spindle lengths of around 1.28 µm (Fig 3c). Given that spindle length and elongation are regulated[16] we asked if spindle length had any correlation to spindle elongation velocity by measuring the spindle elongation velocity as a function of the spindle length of the first point in the time course. We find that the initial length of the nascent spindles has little correlation to the following elongation rate (Fig 3d, Pearson's correlation coefficient r = -0.17), on the other hand the asynchronous WT pre-anaphase populations of spindles decrease in mean elongation velocity as their initial lengths increase (Fig 3d, Pearson's correlation coefficient r = -0.48) and approach the lengths where anaphase occur[6]. These analyses show that the growth immediately following monopolar to bipolar spindle formation is still very stochastic in nature but that once spindle assembly progresses it takes on a very stereotyped elongation regime which slows down as it approaches its target pre-anaphase length.

The forces provided by spindle elongation are essential to bio-orient chromosomes and segregate them, but the stability of the spindle structure is equally as important. Spindle instability and collapse often lead to chromosome attachment defects and loss. We therefore investigated the how the stability of the nascent spindles compared them to the stability of the asynchronous WT pre-anaphase spindles and how this stability evolved during spindle

assembly using spindle length fluctuations as previously reported[6,7]. We find that the nascent spindles exhibit large fluctuations which overlap with the fluctuations of the asynchronous WT spindles of similar mean length (Fig 3e&f). Overall, we find that as spindle assembly progresses from a nascent state towards an anaphase ready spindle, the length fluctuations dampen in a length dependent fashion (Fig 3e & f). We find that the amplitude of spindle length fluctuations of WT nascent bipolar spindles to be similar to that of WT asynchronous spindles of similar lengths (p value > 0.4) (Asynchronous WT mean spindle lengths<1.499 µm, the highest mean nascent spindle length) but that these fluctuations dampen significantly once the spindle lengths increase (p value< $3{\cdot}10^{-8}$ for Asynchronous WT mean spindle lengths>1.499 µm,). Equally, we find that Kinesin-5 sliding contributes to the stability of new bipolar spindles: Cin8-RK kip1Δ and to a lesser extent Cin8-RK (Fig 3 f red) present increased spindle fluctuations compared the WT. We report an increase in spindle fluctuations with increasing kinesin-5 sliding deficiency with Cin8-RK sliding deficient cells exhibiting larger fluctuations than WT (p value < 0.05) and Cin8-RK Kip1Δ (p value = 0.001) exhibiting large fluctuations than both Cin8-RK and WT. Newly formed bipolar spindles are more unstable than longer spindles later in metaphase and are further destabilized in the absence of kinesin-5 sliding.

These data and subsequent analysis of the elongation and stability of nascent spindles reveal that Kinesin-5 sliding is required to ensure that immediately following the monopolar to bipolar spindle transition spindles are stable and sustain net positive elongation. As spindle assembly progresses towards anaphase the system becomes more interconnected and stereotyped as MT overlaps increase, mitotic MAPs deploy, and chromosomes are attached and bioriented. We show that during this assembly process, the nascent bipolar spindles dampen their fluctuations and integrate Kinesin-5 sliding forces to ensure sustained positive elongation. This process of spindles assembly is intrinsically linked with the evolution of the MT architecture of the spindle as it undergoes the transition from a duplicated but unseparated monopolar state to a stereotyped metaphase spindle.

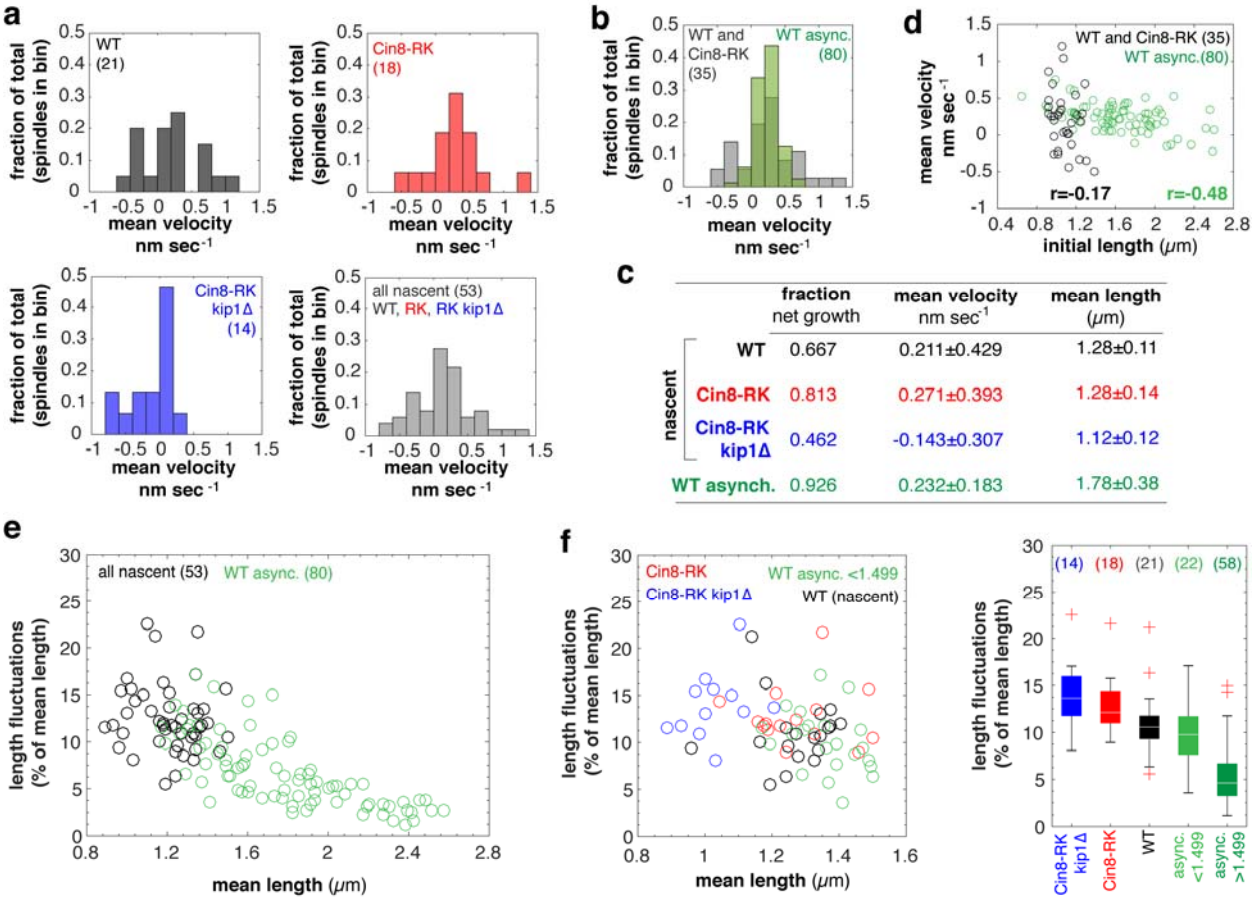

Figure 3 : Kinesin-5 sliding contributes to stability and elongation of nascent spindles. ***a.*** Mean velocities of spindle elongation for nascent WT cells (top left; black n=21), Cin8-RK cells (top right; red n=18) and Cin8-RK Kip1Δ cells (bottom left; blue n=15). The combination of all spindle elongation rates is shown the bottom left panel ***b***. Mean velocity of spindle elongation for nascent WT & Cin8-RK spindles (grey; n=39) and WT asynchronous spindles (green; n=80) ***c.*** Mean velocity of spindle elongation versus initial spindle lengths for nascent WT (black; n=21) and WT asynchronous spindles (green n=80) ***d.*** Table summarising the elongation properties of nascent and asynchronous spindles. ***e.*** Spindle length fluctuations in % of mean length versus mean spindle length for nascent (Black; n=53) and WT asynchronous (Green; n=80) ***f.*** Left panel: Spindle length fluctuations of nascent

Cin8-RK, kip1Δ (blue;n=14), Cin8-RK (red; n=18), WT (black; n=21) and asynchronous WT spindles of mean length inferior to 1.499µm (green; n=22). Right panel: Box plot of spindle length fluctuations.

Microtubule pairing and overlap in monopolar spindles provides insight into the mechanism of bipolar spindle formation by kinesin-5.

The study of microtubule number and pairing using 3D electron tomography has provided many insights into structural changes that occur during spindle assembly and the metaphase to anaphase transition[6,18] but the majority of studies focus on metaphase or anaphase spindles. The MT organization required to initiate the separation of duplicated but unseparated spindle poles (a monopolar spindle) remains unclear and could provide insight into the evolution of spindle elongation and stability during the monopolar to bipolar transition. The nm scale resolution of MT lengths and interactions provided by 3D electron tomography allows us to correlate the system of MTs in the monopolar spindle and the dynamics we have measured for the monopolar to bipolar transition in living cells.

To enrich for wild type cells with monopolar spindles, we used elutriation to prepare samples for 3D electron tomography and were able to reconstruct four monopolar models (duplicated but unseparated poles with interacting MTs). As well, we identified a single 800 nm bipolar spindle, which represents an intermediate stage in metaphase[6,19]. The length of this short bipolar spindle lies between the monopolar state (200 nm) and nascent bipolar state (~1300 nm), with 5% of bipolar spindles with a length of less than 1000 nm after the monopolar to bipolar transition (n=34 of 680 nascent bipolar spindle time points). We reasoned this rare spindle model could provide insight into MT organization in nascent bipolar spindles.

We extracted information for key parameters that describe the microtubule architecture of monopolar spindles; microtubule number, lengths, MT overlap pairings (length and angles). A representative model for a monopolar spindle is shown in Fig 4 a and an early bipolar spindle Fig 4 b. MTs emanating from the same spindle pole are coloured either blue or red. Overlap

regions are shown in white, defined as the contours of MTs from opposing poles separated by ≤ 45nm over ≥ 10nm.

The four tomographic models of monopolar spindles possess between 29 to 61 distinct MT pairs (48.8 ±14 # pairs) with overlap lengths ranging from 11nm to 159 nm (mean overlap 57.7 ± 23.7 nm). The 800 nm bipolar spindle has 48 distinct MT overlap pairs with lengths ranging from 13nm to 434nm (mean overlap 124.1± 104 nm). This contrasts with the length of overlap length of 400 nm is the typical of the ipMTs of metaphase spindles[6,19] . As well, the number of intersecting MT pairs is much greater than the 6-8 ipMTs in metaphase and anaphase spindles[6]. This analysis suggests monopolar spindles lack ipMTs, and that ipMTs have not formed in short bipolar spindles. The overlap profile of the electron tomography models shown in Fig 4a,b are shown in Fig 4 c (top unseparated and bottom early bipolar) with blue and red representing the lengths of each pair of MT from opposing spindle poles and in white the length of the overlap. Results of overlap analysis are summarised in Table 1.

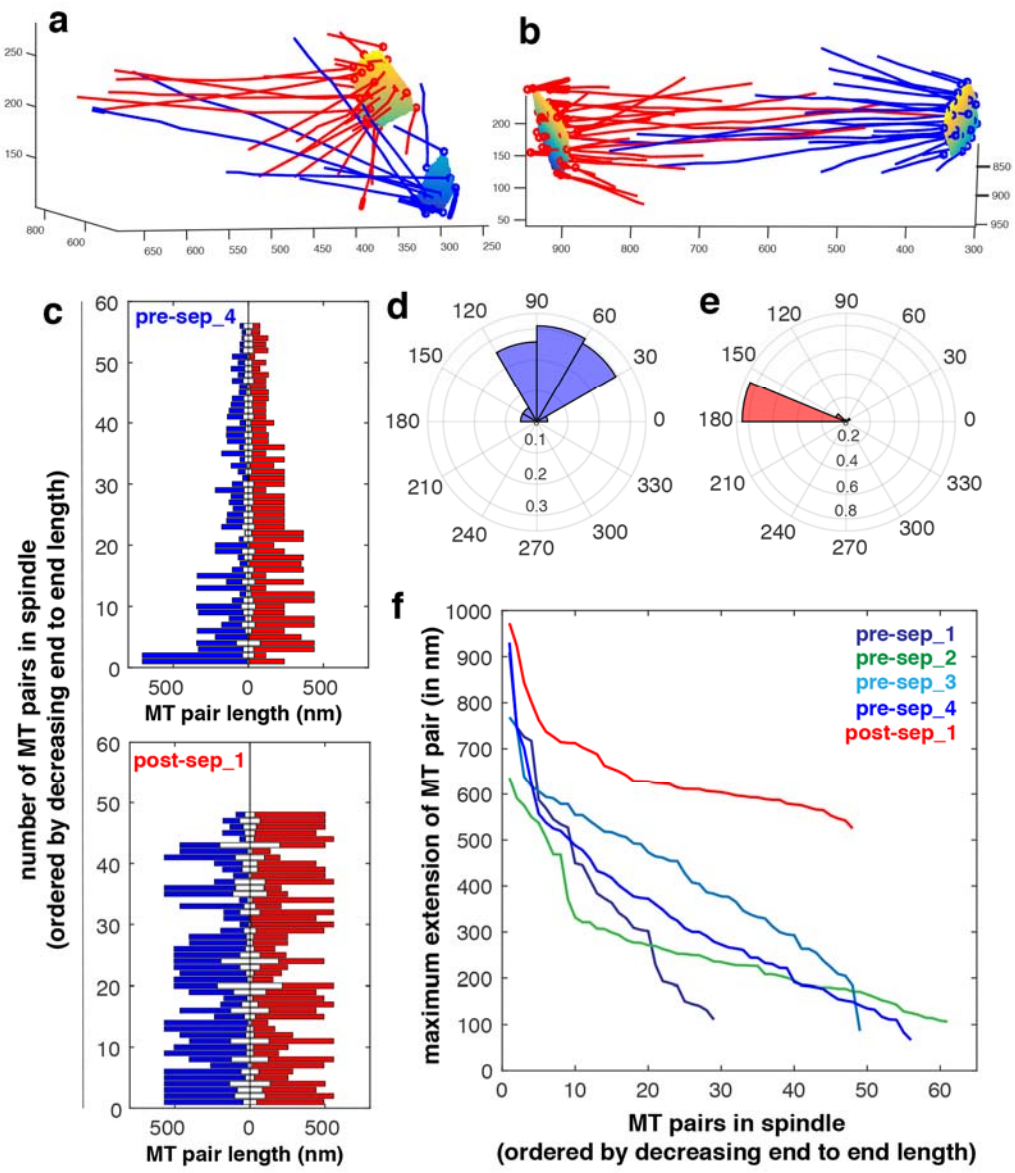

Figure 4: Microtubule architecture of monopolar and short bipolar spindles give insight into Kinesin-5 contributions ***a***. Tomographic reconstruction of a monopolar spindle. ***b.*** Tomographic reconstruction of a short (800 nm) bipolar spindle. For ***a*** and ***b***, MTs of each pole are coloured blue or red. ***c***. Overlap profile of MT pairs. MTs pairings must be spaced <45nm with continuous overlap >10nm. Blue and red indicate MTs from opposite poles, with the overlap region in white. Overlaps are sorted in descending order of total length for a monopolar spindle (top) and bipolar spindle (bottom). Angles of MT pairs presented in a radar plot for the ***d*** monopolar spindles and ***e*** bipolar spindle shown in ***a*** and ***b***

respectively. ***f***. Maximum extension of the MT pairs as defined as the sum of their lengths minus the overlap length are plotted for 4 monopolar spindles and one 800 nm bipolar spindle.

Table I. Parameters for interactions between paired microtubules within monopolar spindles

	monopolar state (n=4)	**bipolar state (800 nm)** (n=1)
overlap number *(n= MT pairs)*	48.8 ±14 (n = 202)	48
mean overlap length (nm) *(n= MT pairs)*	57.7 ± 23.7 (n = 202)	124.1± 104
mean total overlap (µm) *(per spindle)*	2.82 ± 0.85	5.99
mean overlap angle (°) *(n= MT pairs)*	83.0 ± 28.4 (n = 202)	162.3 ± 27.6 (n = 55)

We also characterized the angles formed by the MT overlaps in the monopolar and 800 nm bipolar spindles as their organization is expected to give insight into cross-linking and/or sliding that can be supported by such an architecture. The MT pairs in monopolar spindles present a large range of overlap angles ranging from 30° to 160° but the majority (82%) of pairing angles are between 45° and 120°. In the 800 nm bipolar spindle, the range of angles of MT pairs is more restricted than in the monopolar state, with 81% of MT pairs with angles ranging from 160° to 180° (with 180° being anti-parallel MTs). Representative radar plots of angles formed by MT pairs of the tomogram models in Fig 4 a & b are shown in Fig 4 c. The results of our overlap angle analysis are summarised in Table 1.

Finally, we projected the maximal extension length (MEL) of the MT pairs extracted from the electron tomogram models. The MEL is the length obtained by summing the lengths of the two MTs that form the pair and subtracting the pairs measured overlap length. The MEL provides an upper bound for the length that the pair could extend to, as it disregards where in the MT contour length and the angle the pairing occurs. We plot the MEL for each MT pair for the four monopolar and 800 nm bipolar tomography models in Fig 4 f. The MELs of monopolar spindles range between 600 nm and 900 nm but the vast majority of the MT pairs have a MELs below 500 nm. In contrast, the majority of MELs of the 800 nm bipolar spindle are >600 nm, with a minor set of MELs of 1000 nm; these MT pairs may be compressed. These results illustrate how MTs may be rearranged as a result of bipolar spindle formation. We assume MT crosslinking persists through the monopolar to bipolar spindle formation and that kinesin-5 sliding does not significantly change the overlap length during the transition. With these two assumptions, we use the MELs (Fig 4 f) to estimate the upper bound for the length of a bipolar spindle without the contribution of MT sliding. We approximate an upper bound of 600-900 nm, consistent with the overlap profile of the 800 nm bipolar model (600-1000 nm).

The timing of the transition does not depend on kinesin-5 microtubule sliding

We have shown that the rate and irreversibility of the monopolar to bipolar transition is not significantly altered in the absence of kinesin-5 sliding. Moreover, our analysis of the microtubule architecture of monopolar spindles identified MT pairs with MELs that are consistent with the post-transition lengths of nascent bipolar spindles irrespective of kinesin-5 sliding. Prior to bipolar spindle formation, Cdk1 restrains the proteolysis of kinesin-5. This regulation ensures sufficient kinesin-5 is available to form MT pairs and drive formation of a bipolar spindle[20].

We considered the possibility that the monopolar to bipolar transition may be dependent on a force threshold. If kinesin-5 sliding does contributes to the transition, the accumulation of a high concentration of kinesin-5 motors with attenuated sliding activity may be sufficient to reach

the force threshold required to separate the poles. A compensatory mechanism is expected to delay the onset of the transition in relation to the completion of spindle pole duplication. We therefore investigated if there was a significant cell cycle delay between START and the formation of a bipolar spindle in Cin8-RK and Cin8-RK kip1Δ cells relative to WT cells. START is the point of commitment to enter the cell division cycle, and can be used to benchmark the timing of spindle pole duplication in relation to pole separation, during which kinesin-5 is expected to accumulate on the MTs of monopolar spindles [5,21,22]. We therefore used START as beginning of the process of spindle formation in living cells.

The Whi5 transcriptional repressor is exported from the nucleus at START[21]. We used Whi5-GFP nuclear export to measure the time from START[21] to the monopolar to bipolar transition in single cells. The transition was identified as two resolved spindle poles, with the poles labelled with Spc42-CFP (Fig 3 a). We find the mean delay between START and bipolar spindle formation in WT cells incubated at 25°C is 71.1 ± 23.5 mins (n=67; Fig 5 b). The delay between START and bipolar spindle formation in Cin8-RK cells (64.4 ± 23.5 mins; n=80) and Cin8-RK kip1Δ cells (68.9 ± 22.6 mins; n=88) was not significantly different than that of WT cells (Cin8-RK p=0.07; Cin8-RK kip1Δ p=0.70) (Fig 5 b). We plotted the estimation statistics[23] (Fig 5 c) of the delay as a 95% confidence interval of the mean difference between each dataset, and show the 95% confidence intervals of the bootstrapped mean differences in relation to the WT delay. This suggests that the loss of kinesin-5 sliding does not delay the onset of the monopolar to bipolar transition after commitment to enter the cell cycle. The lack of cell cycle delay along with the monopolar to bipolar transition velocities together suggest that the short but abundant overlaps that are a feature of monopolar spindle support kinesin-5 crosslinking that is required to undergo the monopolar to bipolar transition.

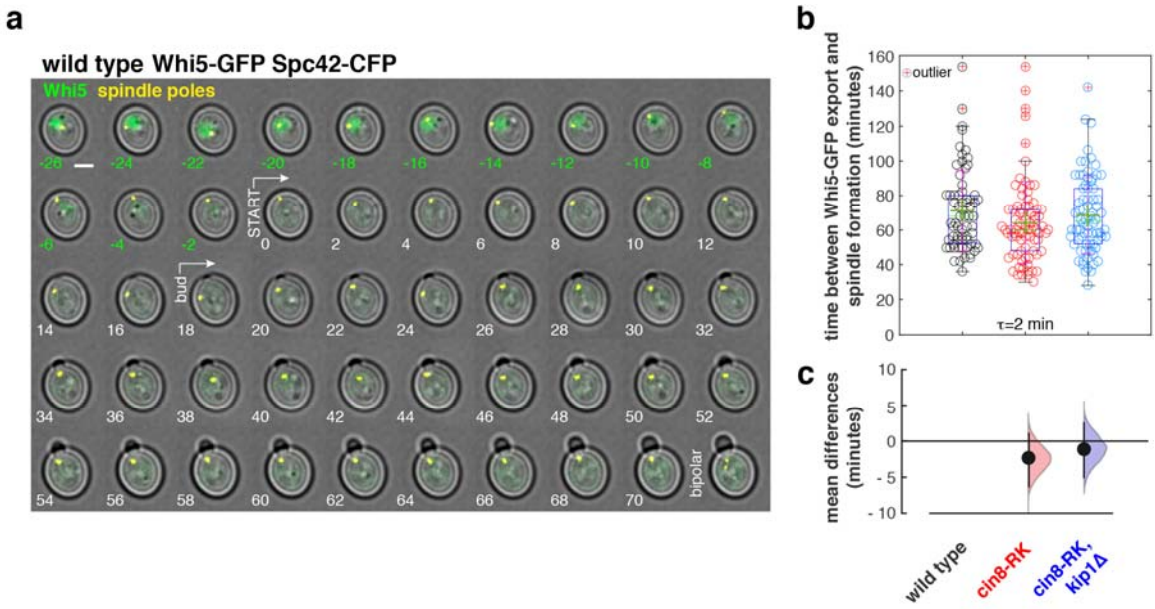

Figure 5: The timing of the monopolar to bipolar spindle transition relative to START is not delayed in the cin8-RK or cin8-RK kip1Δ mutants. ***a***. Time lapse images of WT cells expressing Whi5-GFP showing timescale of nuclear export of Whi5. START (no Whi5-GFP signal in nucleus) and bud emergence are indicated on the timeseries. ***b***. Box plot with data points overlaid for the time delay between START and bipolar spindle formation in WT cells (black n=67), Cin8-RK cells (red n=80) and Cin8-RK Kip1Δ cells (blue n=74). ***c***. Estimation plot of delays as visualized as a bootstrap 95% confidence interval of mean differences.

Kinesin-5 microtubule sliding sets the equilibrium length of nascent bipolar spindles

We have characterized both the velocity and the post transition stability of the formation of a bipolar spindle along with the initial MT architecture that precedes it, but we next wanted to determine if the transition is stereotyped across a population of cells and if so, understand the biological significance of a stereotyped equilibrium length of a new bipolar spindle. The metaphase length of the mitotic spindle is decreased by Kinesin-5 impairment, depletion of Cin8 in particular[2,24]. Cells lacking Cin8 have short metaphase spindles that are likely the result of

partial collapse to the monopolar state, and a metaphase delay due to activation of the spindle assembly checkpoint. These defects are the outcome of the direct role of Cin8 in chromosome congression and kinetochore tension[25].

We investigated whether kinesin-5 sliding contributes to setting a minimum length of nascent bipolar spindles. We binned all the instantaneous spindle lengths for our bipolar spindles formations and plotted them as a histogram. The WT bipolar length distribution (grey n=21 traces) are shown with the Cin8-RK (red = 18 traces) and Cin8-RK Kip1Δ (blue n=15 traces) in Fig 6a. A double gaussian fit is shown for each distribution. The double gaussian fits for the WT, Cin8-RK and Cin8-RK kip1Δ distributions are shown together for comparison (Fig 6 bottom left panel). We find the monopolar state (duplicated unseparated spindle poles) as defined by the peak and width of the gaussian fit for all cells to be consistent with measurements of monopolar spindles in WT cells reported using electron microscopy[19]: 0.24 ± 0.22 um for WT, 0.26 ± 0.26 um for Cin8-RK and 0.28 ± 0.19 um for Cin8-RK kip1Δ.

The contribution of kinesin-5 sliding to setting new bipolar spindle length was apparent when comparing WT cells with an average length of 1.35 ± 0.42 um to Cin8-RK kip1Δ cells with an average length of 1.01 ± 0.54 um. Interestingly, Cin8-RK cells have a spindle length comparable to WT of 1.28 ± 0.54 um, which suggests Kip1 sliding compensates for the Cin8-RK mutation in setting the length of the nascent bipolar spindle.

These results reveal that the equilibration length of nascent bipolar spindles lacking a significant contribution of kinesin-5 (either Cin8 or Kip1), are consistent with the MELs extracted from electron tomography models of monopolar and 800 nm bipolar spindles (Fig 4f) which assume stable MT crosslinking and no MT sliding. Interestingly, we find kinesin-5 sliding ensures the nascent bipolar spindle attains a stereotyped length of 1.3 μm immediately following the transition.

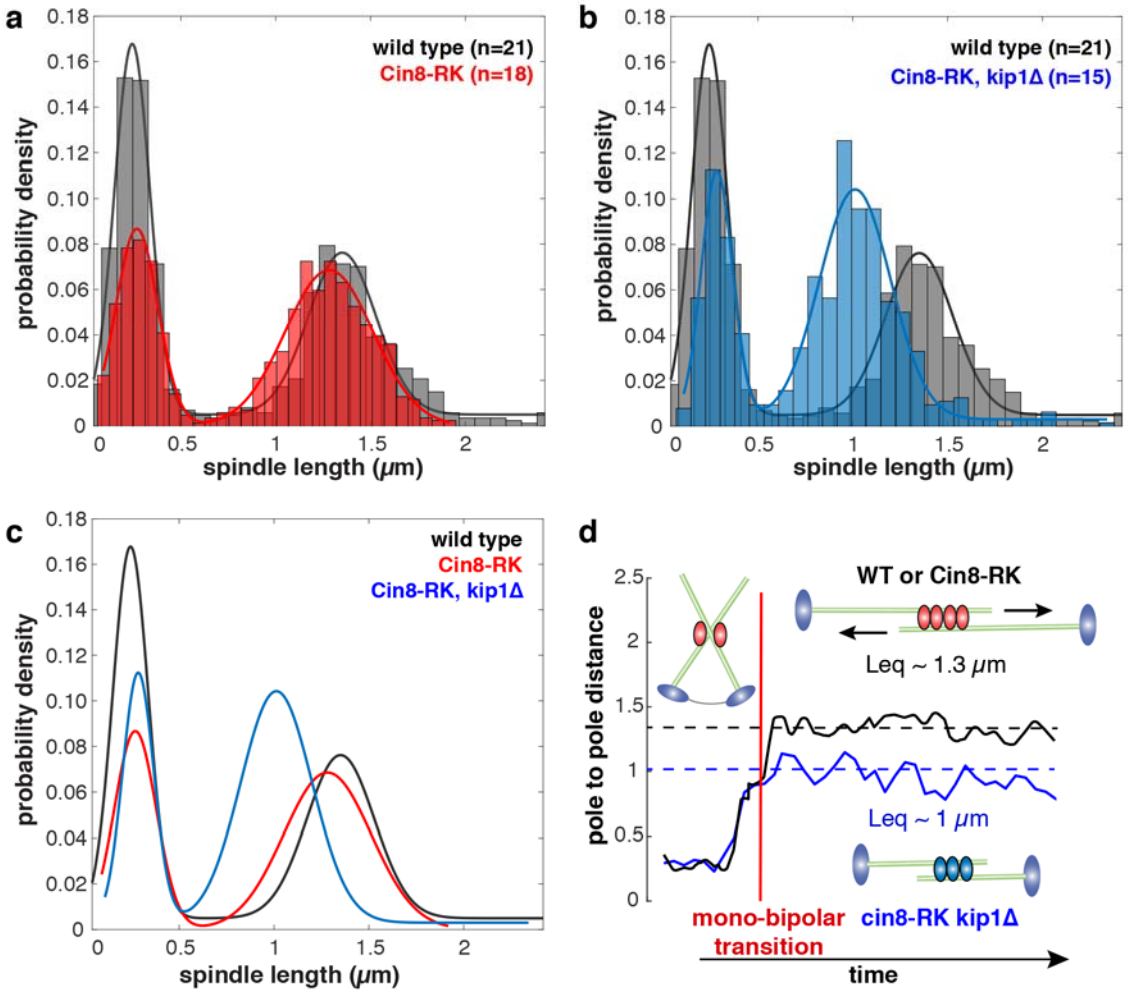

Figure 6: Kinesin-5 sliding sets the equilibrium length of new bipolar spindles *am*. Histogram of the relative probabilities of the spindle lengths during the monopolar to bipolar transition for WT cells (black), Cin8-RK cells (red) and Cin8-RK Kip1Δ cells (blue) with their associated fits to double gaussians. ***c***. Overlay of the fits obtained from the probability distributions shown in ***a*** and ***b***. Diagram of Kinesin-5s contributions to the monopolar to bipolar spindle formation and later mitosis. Kinesin-5 crosslinking enacts a fast, irreversible and stereotyped transition from monopolar to bipolar spindle. Kinesin-5 sliding then ensures that the equilibration length of the new spindle is sufficient to enact tension forces to correctly attach chromosomes and progress through mitosis.

Discussion

The monopolar to bipolar transition is a fast and irreversible process that produces a stable bipolar spindle.

In this study, we demonstrate for the first time that the transition from a monopolar spindle to a bipolar spindle is both faster than any other step in spindle assembly including anaphase. We report that once a bipolar spindle is formed, it remains bipolar and does not collapse back to a monopolar state, thus spindle formation is a two-state irreversible transition. Using mutations in the two kinesin-5 orthologs of budding yeast, we have dissected out the contributions of kinesin-5 crosslinking and sliding modalities to the monopolar to bipolar transition. We found that the crosslinking modality of kinesin-5 is sufficient for fast and irreversible formation of a bipolar spindle. We have shown that Kinesin-5 sliding nonetheless contributes to the specifying the equilibration length of the nascent bipolar spindle as previously suggested[26] and dampening its fluctuations. These the dampening of the spindle fluctuations occurs all through metaphase spindle assembly up until anaphase. We equally show that the nascent bipolar spindles require Kinesin-5 to start undergoing net elongation towards the anaphase onset spindle lengths. The nature of this net elongation switches from a stochastic noisy regime in the nascent spindles to a stereotyped elongation regime as metaphase progresses only to slow down at the approach of anaphase onset lengths. Together our results highlight Kinesin-5 crosslinking as the driver of the formation of nascent bipolar spindles and sufficient to prevent their collapse but Kinesin-5 sliding as required to fully damp the spindles fluctuations and allow it to undergo stereotyped elongation towards anaphase onset lenghts.

Force generation during and after the monopolar to bipolar transition illustrates the importance of both cross-linking and sliding modalities of Kinesin-5 in spindle assembly

Combining our study of the microtubule architecture and our characterization of the role of kinesin-5 cross-linking in the monopolar to bipolar spindle transition has provided us with a

comprehensive outlook on the sources of force generation for this transition. Our study has shown that the monopolar spindle contains many short and/or high angle (> 30˚) anti-parallel MT pairs. Cin8 appears to be particularly well suited to crosslink MTs across this diverse and challenging set of pairing architectures found in monopolar spindles[27] thanks to its non-canonical MT binding sites[28]. Cin8 also possesses a nonmotor MT binding site that is required for crosslinking as it increases its affinity to MTs independent of motor forces[29]. Cin8 has also been found to cluster near the poles of the monopolar spindles which puts it in a position capture and crosslink MTs from the opposing pole[30].

However, in the monopolar state the overlap length of MT pairs are often short (>100nm) and not expected to support cooperative Kinesin-5 sliding responsible for the large anaphase spindle elongations[27,31]. These high angle crosslinks have been found to be able to enact measurable deflection forces[27] which if summed across many MT pairs as present in monopolar spindles could provide a considerable pushing force to separate the spindle poles. Individual Kinesin-5 motors on a crosslinked MT have been found to apply approximately 1.5 pN to the MT[27]. Our analysis of the MT organization within monopolar spindles shows up to 50 paired MTs, each of which will be crosslinked by Kinesin-5 motors. This could sum to forces in the hundreds of pNs range which is comparable to those during maximal pole separation[32].

Kinesin-5 and the structural MAP Ase1 both stabilize bipolar spindles through MT crosslinking[33]. In budding yeast, loss of Ase1 increases the frequency of spindle collapse in anaphase[34]. Ase1 also functions to stabilize metaphase spindles. In both fission and budding yeasts, MT crosslinking appears to be sufficient for formation of a bipolar spindle. In fission yeast, Ase1 cross-linking alone supports bipolar spindle formation in the absence of both kinesin-5 and the minus end directed motor kinesin 14[4]. In budding yeast, overexpression of Ase1 in G1 can supports the formation of a bipolar spindle in the absence of both Cin8 and Kip1[5], however these cells are inviable. This suggests that in budding yeast, MT cross-linking by Ase1 alone cannot support the formation of a functional bipolar spindle. Our finding that kinesin-

5 MT sliding is important for the nascent bipolar spindle to attain a stereotyped equilibrium length is consistent with Ase1 playing a minor and or partially redundant role in spindle formation in budding yeast. Together with our findings, these studies reinforce the important role of MT cross-linking by kinesin-5 in the formation of the eukaryotic bipolar spindle. Nevertheless, a detailed analysis that investigates Ase1's potential contributions to the monopolar to bipolar transition and the stability nascent spindles will be an important step towards fully understanding the mechanism for fast, irreversible formation of a stable bipolar spindle in budding yeast.

In both animal and fungal cells, the duplicated spindle poles of the monopolar spindle are tethered by a linker which must be cleaved in order to form a bipolar spindle. Cleavage of the linker structure therefore has a major role in regulating the progression of mitosis via the monopolar to bipolar transition. The full composition of the spindle pole linker is still unclear, but contains proteins conserved among eukaryotes including centrin and the coiled-coil protein Sfi1 (hSfi1 in human cells). Intriguingly the Sfi1 protein has been implicated in restricting one round of pole duplication per cell cycle via phospho-regulation of its C terminus[35,36]. Sfi1 C termini dimerize C-C to form a discrete linker between duplicated but unseparated spindle pole bodies which places them at an important junction to regulate bridge cleavage and spindle pole separation. Sfi1 C-terminus phospho-regulation has been implicated in delaying and altogether blocking Sfi1 dimer dissociation in budding yeast, implying a mechanism that regulates the cleavage of the half bridge structure might sense force.

The force acting on the half bridge could produce the tension that is required for Sfi1 dimer dissolution. The half bridge could store tension that is released when the threshold is met for monopolar to bipolar spindle transition. This threshold requires sufficient kinesin-5 cross-linking occurred to trigger the transition. The accumulation of forces on the linker up to a certain threshold in combination with cell cycle related phosphor regulation could provide an interesting

novel tension sensing mechanism employed by the spindle and could explain the bimodal step like transition we observe for the monopolar to bipolar transition for all our kinesin-5 mutants.

An irreversible transition to a stable and stereotyped bipolar state is important for subsequent steps in mitosis

Kinesin-5 has diverse roles in mitosis, arising from its ability to cross-link and slide MT. Its processive plus ended sliding of ipMTs has been seen as the main driver of spindle elongation and as a result chromosome segregation[37]. But recent studies have revelled a plethora of different properties and roles for Kinesin-5, namely possesses additional non-canonical MT binding sites[28,29] in addition to binding sites in the motor domain required for motility[10,31,38,39]. Kinesin-5 also localizes to the kinetochore-MT interface and acts as a length dependent depolymerase to facilitate chromosome congression[24] and recruits PP1 to kinetochores, contributing to maintaining Ndc80 attachment to microtubules and tension generation[25]. Our study reveal that a essential step in mitotic spindle assembly that had been previously overlooked as simply a result of Kinesin-5's sliding modality in fact integrates both its sliding and crosslinking modality to produce a stable and elongating metaphase spindle. In all cell types the length of the metaphase spindle is stereotyped to the volume of the cells[16]. Maintaining this length is the result of the balanced interplay between many actors, and in balance arising from MT dynamics, kinetochore attachments or microtubule associated proteins can severely affect the faithful segregation of genetic material.

Stable spindle bipolarity is essential for correct chromosome attachment in mitosis[40,41] and meiosis[42]. The mechanisms by which cells sense and maintain correct MT-kinetochore attachments rely on both attachment and tension, but maintaining the bipolar state is the first

and most important requirement[43,44]. Correct chromosome attachment is a noisy and stochastic process sensitive to small defects in MT dynamic instabilities and the interactions between the many protein complexes that govern the kinetochore-MT interface[45,46]. Spindle collapse is expected to severely impair mechanisms for stabilizing kinetochore-MT attachments emanating from opposing poles. In a collapsed spindle, the likelihood of syntelic and merotelic attachments increases due to the proximity of MTs emanating from both poles[41]. When kinesin-5 Eg5 is inhibited by monastral, chromosome dispersion (a measure of defective chromosome congression) is maximal when metaphase spindle length is reduced by only 35%[15].

The threshold between pathological spindle instability leading to chromosome loss and "physiological" instability that is characteristic of nascent bipolar spindles is unclear. The intrinsic instability of the nascent bipolar spindle is not captured in the dynamic models used to understand of the chromosome search and capture mechanism, which assume that the positions of the spindle poles are static when simulating MT dynamics, kinetochore-MT attachments and chromosome movements[47-49]. The stereotyped length of nascent bipolar spindles provides insight into the dual role of kinesin-5 in setting the length threshold. Our findings reveal that coupling kinesin-5 cross-linking and MT sliding during the earliest steps in spindle formation ensures a rapid transition to a stable bipolar state that supports the efficient search and capture of kinetochores as well as a sufficient length for tension to be applied to bioriented chromosomes.

Materials and Methods

Strain construction and cell culture conditions

All yeast strains are derivatives of BY4741. Mutant form of Cin8 (cin8-3) was generated in plasmid pSU19 using the USER cloning (New England Biolabs) [50] PCR amplified and integrated into the CIN8 locus by homologous recombination. The resulting strain was crossed with a haploid strain which carries the Fluorophore switching cassette, loxP-mCherry-KanMx4-loxP-GFP His3-MX6[9]. The haploids bearing CIN8-R196K in combination with the fluorophore- switching cassette were isolated by tetrad dissection. The conditional estradiol inducible Cre recombinase from pYB1109[9] was randomly integrated into the genome of EN15 and YV1085 by transformation resulting in EN1 and YV1099 strains, respectively. EN1, YV1099 and YB1037 strains were used for microscopy.

Live cell microscopy

Yeast strains were grown to log phase (OD_600 ~0.1-0.6) in synthetic complete (SC) media supplemented with 2mM ascorbate at 25˚C. All live cell imaging was undertaken at 25˚C.

For bipolar spindle formation and fluorophore switching technique Cre recombinase induction was used, β-Eestradiol (1μM) was added to SC media 120 min before imaging. Cells were prepared for imaging as previously reported[6,7]

Bipolar spindle formation was imaged on a Quorum Diskovery platform installed on a Leica DMi8 inverted microscope. This system consists of a HCX PL APO 100x/1.47 OIL CORR TIRF objective (Leica), an DISKOVERY multi-modal imaging system (Spectral) with a multi-point confocal 50um pinhole spinning disk and dual iXon Ultra 512x512 EMCCD (Andor) cameras for simultaneous imaging, ASI three axis motorized stage controller, and MCL nano-view piezo

stage, 488nm and 561nm solid state OPSL lasers linked to a Borealis beam conditioning unit. Image acquisition and microscope control was executed using MetaMorph (Molecular Devices). Images were acquired in stream mode, with each 6 µm z-stack composed of 30 z-slices of 200 nm, and an exposure time of 50 ms. Cells were imaged for 20 mins with a 20 s time step (τ) between stack acquisitions (60 time points).

To measure the timing of bipolar spindle relative to START, early log phase cells (OD600 0.1-0.3) were concentrated and spotted onto a pad of 1% agarose SC contained in a gene frame (ThermoScientific). Cells were incubated on the agar pad/slide for 10 mins at ambient temperature (~25˚ C) before imaging. Imaging data was taken on Olympus IX83 microscope using 100x oil objective lens (Olympus Plan Apo 100X NA 1.40 oil). Images were captured using a Hamamatsu Orca-Flash 4.0 sCMOS camera. Z-stacks were done using a NanoScanZ piezo by Prior Scientific. Excitation was undertaken using an X-Cite 120 LED lamp using the ET–ECFP/EYFP/mCherry filter set (Chroma). Olympus CellSens 2.1 imaging software was used to control the microscope, illumination and acquisition. Images were collected as 5 µm Z-stacks (10 slices of 0.5 µm) with exposure time of 100 ms. Cells were imaged for 4 hours with a 2 min τ between stack acquisitions (120 timepoints). The 2 min τ was selected based on the ~ 90 sec timescale of the monopolar to bipolar transition (Fig. 1

Analysis of bipolar spindle formation and spindle stability

Pole finding and tracking was implemented in a custom GUI in Matlab using previously implemented algorithms[6,7]. Briefly individual yeast cells were segmented using a seeded watershed algorithm, then SPs were fit to 3D gaussians and tracks were made using Hungarian based particle linking. The dual cameras were first aligned using TetraSpeck microspheres, and then chromatic shift and camera shift was measured and corrected for in the analysis.

Bipolar spindle transition velocities were computed by determining the local maxima/minima of the acceleration curves of the spindle lengths to determine start and end points of the transitions and then computing spindle formation velocity.

As previously measured spindle fluctuations[7] are computed as the standard deviation of the instantaneous spindle lengths post bipolar spindle formation as determined by the end point of the transition. Spindle fluctuations are normalized by dividing their fluctuations by their mean spindle lengths over the time course. Nascent and asynchronous spindle elongation were computed by first meaning instantaneous spindle lengths with a 3-point sliding window and then using a linear regression on the data. The slope of the linear fit is used as the mean velocity of the spindle over the timecourse.

Spindle equilibrium was visualized using relative probability 30 bin histograms. The probabilities where then fit to a double gaussian distribution to obtain the two equilibrium distributions: pre-separation and post-separation.

The cumulative distribution was computed as the length of the midpoint of the bipolar spindle formation as determined by the start and end points for the velocities.

Analysis of delay between START and bipolar spindle formation using Whi5-GFP

Whi5-GFP nuclear export was used to identify START in G1 (unbudded) cells[21]. Spc42-CFP was used to detect the spindle poles. Image z-stacks are max projected in FIJI. START was determined by visual inspection as the first time point where the nuclear Whi5-GFP fluorescence signal was indistinguishable from that found in the cytoplasm. We determined that point to be START, as it is the completion of Whi5 export from the nucleus to the cytoplasm.

The time delay until bipolar spindle formation was determined as the time elapsed between START and the first timepoint where two distinct spindle poles foci could be resolved.

Electron tomography of monopolar spindles

Electron tomography was performed in collaboration with Eileen O'Toole and Mark Winey at the University of Colorado, Boulder. Unbudded (G1) cells were enriched using centrifugal elutriation on a Beckman Coulter Avanti system. Briefly, 200 mL yeast cultures were grown in YPD to an OD600 of 0.5. This culture was concentrated and injected into the centrifugal elutriator. Cells were separated using a flow rate of seven millilitres per minute and a centrifuge rotor speed of 1100 RPM. Fractions were collected every ten minutes and checked under the microscope for enrichment of unbudded cells. Fractions enriched for unbudded cells were then used to make resin-embedded tomography sections at the FEMR (McGill University). Cells from enriched fractions were collected by vacuum filtration and scraped into a 0.1 mm brass planchette. Cells were then vitrified using a Leica Microsystems EM PACT2 High Pressure Freezer System. Afterwards, cells were removed from the planchette and underwent freeze-substitution using a solution of 0.25% glutaraldehyde/0.1% uranyl acetate in 100% acetone[51]. Cells were then embedded in Lowicryl HM20, and polymerized with UV radiation at -45°C using a Leica Microsystems EM AFS2. Resin-embedded cells were cut into serial sections, collected onto slot grids, stained at the University of Colorado, Boulder and tomography performed as previously described[51]. Monopolar spindle models were reconstructed from tomographs using the IMOD software package[52,53]. Microtubule pairing analysis was performed using MatLab (MathWorks, Natick, MA). Pairwise distances between microtubule contour lengths were computed and overlaps defined as regions separated by ≤ 45nm over a length of ≥10nm as defined in previous studies[6]. Overlap angles were computed from vectors formed by the start and end of the overlap region of each microtubule pair in order to account for bent microtubules.

Author contributions

A.L. Conceived of the project, contributed to the cre-lox experiments and analysis, performed Whi5 delay experiments and analysis and contributed to the EM spindle analysis. Wrote the manuscript.

E.N. Conceived of the project and contributed cre-lox experiments and analysis.

S.S. Contributed to monopolar EM spindle architecture analysis

K.S. Contributed to EM tomography of monopolar spindles

P.F. Contributed and supervised the data analysis and edited the manuscript.

J.V. Conceived of and supervised the project, coordinated the experiments, and wrote the manuscript.

Acknowledgements

The authors thank members of the Vogel lab, Steph Weber and Susanne Bechstedt for discussions and their comments on the manuscript, the Integrated Quantitative Biology Initiative for access to the confocal microscope, the FEMR facility at McGill University for access to high pressure freezing equipment used to prepare cells for monopolar spindle EM tomography. Tomography was performed with Eileen O'Toole at the Boulder Electron Microscopy Services at the University of Colorado, Boulder. AL is supported by fellowships from the Cellular Dynamics of Macromolecular Complexes training program (Natural Sciences and Engineering Research Council of Canada) and the Fonds Nature et technologies Quebec (FRQNT). This research was supported by a grant from the Canadian Institutes of Health Research (MOP-123335) to JV, a FQRNT team grant (G241608) to PF and JV, and an Innovation Fund infrastructure grant (33122) from the Canadian Foundation for Innovation to JV.

REFERENCES

1 Kashina, A. S., Scholey, J. M., Leszyk, J. D. & Saxton, W. M. An essential bipolar mitotic motor. *Nature* **384**, 225, doi:10.1038/384225a0 (1996).

2 Straight, A. F., Sedat, J. W. & Murray, A. W. Time-lapse microscopy reveals unique roles for kinesins during anaphase in budding yeast. *J Cell Biol* **143**, 687-694 (1998).

3 Hoyt, M., He, L., Loo, K. & Saunders, W. Two Saccharomyces cerevisiae kinesin-related gene products required for mitotic spindle assembly. *The Journal of cell biology* (1992).

4 Rincon, S. A. *et al.* Kinesin-5-independent mitotic spindle assembly requires the antiparallel microtubule crosslinker Ase1 in fission yeast. *Nat Commun* **8**, 15286, doi:10.1038/ncomms15286 (2017).

5 Crasta, K., Huang, P., Morgan, G., Winey, M. & Surana, U. Cdk1 regulates centrosome separation by restraining proteolysis of microtubule-associated proteins. *EMBO J.* **25**, 2551-2563 (2006).

6 Nazarova, E. *et al.* Distinct roles for antiparallel microtubule pairing and overlap during early spindle assembly. *Mol Biol Cell* **24**, 3238-3250 (2013).

7 Shulist, K. *et al.* Interrogation of □-tubulin alleles using high-resolution fitness measurements reveals a distinct cytoplasmic function in spindle alignment. *Sci. Reports* **7**, doi:10.1038/s41598-017-11789-7 (2017).

8 Verzijlbergen, K. F. *et al.* Recombination-induced tag exchange to track old and new proteins. *Proc Natl Acad Sci U S A* **107**, 64-68, doi:10.1073/pnas.0911164107 (2010).

9 Hotz, M. *et al.* Spindle pole bodies exploit the mitotic exit network in metaphase to drive their age-dependent segregation. *Cell* **148**, 958-972 (2012).

10 Adina, G.-G. *et al.* Directionality of individual kinesin-5 Cin8 motors is modulated by loop 8, ionic strength and microtubule geometry. *EMBO J.* **30**, 4942-4954 (2011).

11 Gheber, L., Kuo, S. & Hoyt, M. Motile properties of the kinesin-related Cin8p spindle motor extracted from Saccharomyces cerevisiae cells. *J. Biol. Chem.* **274**, 9564-9572 (1999).

12 van Heesbeen, R. G., Tanenbaum, M. E. & Medema, R. H. Balanced activity of three mitotic motors is required for bipolar spindle assembly and chromosome segregation. *Cell Rep* **8**, 948-956, doi:10.1016/j.celrep.2014.07.015 (2014).

13 Kashina, A. S. *et al.* A bipolar kinesin. *Nature* **379**, 270-272, doi:10.1038/379270a0 (1996).

14 Kapitein, L. C. *et al.* The bipolar mitotic kinesin Eg5 moves on both microtubules that it crosslinks. *Nature* **435**, 114-118, doi:10.1038/nature03503 (2005).

15 Kapoor, T. M., Mayer, T. U., Coughlin, M. L. & Mitchison, T. J. Probing spindle assembly mechanisms with monastrol, a small molecule inhibitor of the mitotic kinesin, Eg5. *J Cell Biol* **150**, 975-988 (2000).

16 Goshima, G. & Scholey, J. M. Control of mitotic spindle length. *Annu. Rev. Cell Dev. Biol.* **26**, 21-57 (2010).

17 Straight, A. F., Marshall, W. F., Sedat, J. W. & Murray, A. W. Mitosis in living budding yeast: anaphase A but no metaphase plate. *Science* **277**, 574-578 (1997).

18 ET, O. T., Winey, M. & JR, M. High-voltage electron tomography of spindle pole bodies and early mitotic spindles in the yeast Saccharomyces cerevisiae. (1999).

19 Winey, M. *et al.* Three-dimensional ultrastructural analysis of the Saccharomyces cerevisiae mitotic spindle. (1995).

20 Crasta, K., Lim, H. H., Giddings, T. H., Jr., Winey, M. & Surana, U. Inactivation of Cdh1 by synergistic action of Cdk1 and polo kinase is necessary for proper assembly of the mitotic spindle. *Nat Cell Biol* **10**, 665-675, doi:10.1038/ncb1729 (2008).

21 Skotheim, J. M., Di Talia, S., Siggia, E. D. & Cross, F. R. Positive feedback of G1 cyclins ensures coherent cell cycle entry. *Nature* **454**, 291-296 (2008).

22 Kraikivski, P., Chen, K. C., Laomettachit, T., Murali, T. M. & Tyson, J. J. From START to FINISH: computational analysis of cell cycle control in budding yeast. *NPJ Syst Biol Appl* **1**, 15016, doi:10.1038/npjsba.2015.16 (2015).

23 Gardner, M. J. & Altman, D. G. Confidence intervals rather than P values: estimation rather than hypothesis testing. *Br Med J (Clin Res Ed)* **292**, 746-750 (1986).

24 Gardner, M. K. *et al.* Chromosome congression by Kinesin-5 motor-mediated disassembly of longer kinetochore microtubules. *Cell* **135**, 894-906 (2008).

25 Suzuki, A. *et al.* A Kinesin-5, Cin8, Recruits Protein Phosphatase 1 to Kinetochores and Regulates Chromosome Segregation. *Curr Biol*, doi:10.1016/j.cub.2018.08.038 (2018).

26 Straight, A., Sedat, J. & Murray, A. Time-lapse microscopy reveals unique roles for kinesins during anaphase in budding yeast. *J. Cell Biol.* **143**, 687-694 (1998).

27 Shimamoto, Y., Forth, S. & Kapoor, T. M. Measuring Pushing and Braking Forces Generated by Ensembles of Kinesin-5 Crosslinking Two Microtubules. *Dev. Cell* **34**, 669-681 (2015).

28 Bell, K. M., Cha, H. K., Sindelar, C. V. & Cochran, J. C. The yeast kinesin-5 Cin8 interacts with the microtubule in a noncanonical manner. *J Biol Chem* **292**, 14680-14694, doi:10.1074/jbc.M117.797662 (2017).

29 Weinger, J. S., Qiu, M., Yang, G. & Kapoor, T. M. A nonmotor microtubule binding site in kinesin-5 is required for filament crosslinking and sliding. *Curr Biol* **21**, 154-160, doi:10.1016/j.cub.2010.12.038 (2011).

30 Shapira, O., Goldstein, A., Al-Bassam, J. & Gheber, L. A potential physiological role for bi-directional motility and motor clustering of mitotic kinesin-5 Cin8 in yeast mitosis. *J Cell Sci* **130**, 725-734, doi:10.1242/jcs.195040 (2017).

31 Roostalu, J. *et al.* Directional switching of the kinesin Cin8 through motor coupling. *Science* **332**, 94-99 (2011).

32 Cytrynbaum, E. N., Scholey, J. M. & Mogilner, A. A force balance model of early spindle pole separation in Drosophila embryos. *Biophys J* **84**, 757-769, doi:10.1016/S0006-3495(03)74895-4 (2003).

33 Khmelinskii, A., Roostalu, J., Roque, H., Antony, C. & Schiebel, E. Phosphorylation-dependent protein interactions at the spindle midzone mediate cell cycle regulation of spindle elongation. *Dev. Cell* **17**, 244-256 (2009).

34 Schuyler, S. C., Liu, J. Y. & Pellman, D. The molecular function of Ase1p: evidence for a MAP-dependent midzone-specific spindle matrix. Microtubule-associated proteins. *J Cell Biol* **160**, 517-528, doi:10.1083/jcb.200210021 (2003).

35 Elserafy, M. *et al.* Molecular Mechanisms that Restrict Yeast Centrosome Duplication to One Event per Cell Cycle. *Curr. Biol.* **24**, 1456-1466 (2014).

36 Seybold, C. *et al.* Kar1 binding to Sfi1 C-terminal regions anchors the SPB bridge to the nuclear envelope. *J Cell Biol* **209**, 843-861, doi:10.1083/jcb.201412050 (2015).

37 Stephens, A. D. *et al.* Individual pericentromeres display coordinated motion and stretching in the yeast spindle. *J Cell Biol* **203**, 407-416, doi:10.1083/jcb.201307104 (2013).

38 Fridman, V. *et al.* Kinesin-5 Kip1 is a bi-directional motor that stabilizes microtubules and tracks their plus-ends in vivo. **126**, 4147-4159 (2013).

39 Edamatsu, M. Bidirectional motility of the fission yeast kinesin-5, Cut7. *Biochem Biophys Res Commun* **446**, 231-234, doi:10.1016/j.bbrc.2014.02.106 (2014).

40 Tanenbaum, M. E. & Medema, R. H. Mechanisms of centrosome separation and bipolar spindle assembly. *Dev Cell* **19**, 797-806, doi:10.1016/j.devcel.2010.11.011 (2010).

41 Tanaka, T. U. Kinetochore-microtubule interactions: steps towards bi-orientation. *EMBO J* **29**, 4070-4082, doi:10.1038/emboj.2010.294 (2010).

42 Segbert, C. *et al.* KLP-18, a Klp2 kinesin, is required for assembly of acentrosomal meiotic spindles in Caenorhabditis elegans. *Mol Biol Cell* **14**, 4458-4469, doi:10.1091/mbc.e03-05-0283 (2003).

43 Musacchio, A. & Salmon, E. D. The spindle-assembly checkpoint in space and time. *Nat. Rev. Mol. Cell Biol.* **8**, 379-393 (2007).

44 Pinsky, B. A. & Biggins, S. The spindle checkpoint: tension versus attachment. *Trends Cell Biol* **15**, 486-493, doi:10.1016/j.tcb.2005.07.005 (2005).

45 Gay, G., Courtheoux, T., Reyes, C., Tournier, S. & Gachet, Y. A stochastic model of kinetochore-microtubule attachment accurately describes fission yeast

chromosome segregation. *J Cell Biol* **196**, 757-774, doi:10.1083/jcb.201107124 (2012).

46 Maiato, H., DeLuca, J., Salmon, E. D. & Earnshaw, W. C. The dynamic kinetochore-microtubule interface. *J Cell Sci* **117**, 5461-5477, doi:10.1242/jcs.01536 (2004).

47 Paul, R. *et al.* Computer simulations predict that chromosome movements and rotations accelerate mitotic spindle assembly without compromising accuracy. *Proc Natl Acad Sci U S A* **106**, 15708-15713, doi:10.1073/pnas.0908261106 (2009).

48 Wollman, R. *et al.* Efficient chromosome capture requires a bias in the 'search-and-capture' process during mitotic-spindle assembly. *Curr Biol* **15**, 828-832, doi:10.1016/j.cub.2005.03.019 (2005).

49 Vasileva, V. *et al.* Molecular mechanisms facilitating the initial kinetochore encounter with spindle microtubules. *J Cell Biol* **216**, 1609-1622, doi:10.1083/jcb.201608122 (2017).

50 Bitinaite, J. *et al.* USER™ friendly DNA engineering and cloning method by uracil excision. *Nucleic acids research* **35**, 1992-2002 (2007).

51 O'Toole, E. T., Winey, M., McIntosh, J. R. & Mastronarde, D. N. Electron tomography of yeast cells. *Methods Enzymol* **351**, 81-95 (2002).

52 Kremer, J. R., Mastronarde, D. N. & McIntosh, J. R. Computer visualization of three-dimensional image data using IMOD. *J Struct Biol* **116**, 71-76, doi:10.1006/jsbi.1996.0013 (1996).

53 Mastronarde, D. N. Dual-axis tomography: an approach with alignment methods that preserve resolution. *J Struct Biol* **120**, 343-352, doi:10.1006/jsbi.1997.3919 (1997).